Electronic Supplementary Material (ESI) for Inorganic Chemistry Frontiers.

Lithium Nickel Borides: evolution of [NiB] layers driven by Li pressure

Volodymyr Gvozdetskyi,[a] Yang Sun,[d] Xin Zhao,[b] Gourab Bhaskar,[a] Scott L. Carnahan,[a,b] Colin P. Harmer,[a,b] Feng Zhang,[b] Raquel A. Ribeiro,[c] Paul C. Canfield,[b,c] Aaron J. Rossini,[a,b] Cai-Zhuang Wang,[b,c] Kai-Ming Ho,[c] Julia V. Zaikina[a]

[a] *Department of Chemistry, Iowa State University, Ames, Iowa 50011, United States*

[b] *Ames Laboratory, US DOE, Iowa State University, Ames, Iowa 50011, United States*

[c] *Department of Physics and Astronomy, Iowa State University, Ames, Iowa 50011, United States*

[d] *Department of Applied Physics and Applied Mathematics, Columbia University, New York, NY, 10027, USA*

Supporting Information

Table of Contents

Table S1. Experimental details and crystallographic data for two structure models of the *RT*-$Li_{1+x}NiB$ structure: monoclinic *RT(m),* derived from the parent *RT(m)*-LiNiB, and triclinic *RT(t)* with extra Li atoms within the layer. Rietveld refinement was performed on data collected using high resolution synchrotron powder X-ray diffraction (11-BM-B APS).

Empirical formula	*RT(m)*-$Li_{1+x}NiB^{*}$		*RT(t)*-$Li_{1+x}NiB^{**}$	
Formula weight, g/mol	76.45		77.61	
Space group, *Z*	$P2_1/c$, 16		*P*1,48	
Cell parameters:				
a, Å	18.277(1)	18.209(1)	18.2763(4)	18.2088(4)
b, Å	4.86606(5)	4.86137(3)	4.86589(3)	4.86134(3)
c, Å	6.1818(2)	6.1754(2)	18.5447(5)	18.5264(4)
α, °			89.9810(6)	89.9808(9)
β, °	107.623(1)	107.542(1)	107.6202(9)	107.5434(9)
γ, °			90.056(2)	90.067(2)
V, $Å^3$	524.00(2)	521.23(1)	1571.82(3)	1563.67(3)
Temperature, K	295	100	295	100
Wavelength, Å	λ = 0.412815			
Step scan	0.001			
2*θ*° range	1-50			
Program	GSAS II			
R_B	0.15	0.15	0.15	0.14
R_P	0.13	0.12	0.13	0.12
G.O.F.	4.08	3.82	3.88	3.64

*– Further details can be obtained from Cambridge Crystallographic Data Centre/FIZ Karlsruhe deposition service on quoting the depository number CSD-2031390 (100 K) and CSD-2031382 (295 K).

**– Further details can be obtained from Cambridge Crystallographic Data Centre/FIZ Karlsruhe deposition service on quoting the depository number CSD-2031387 (100 K) and CSD-2031379 (295 K).

Table S2. Atomic coordinates and isotropic equivalent displacement parameters of the *RT(m)*-$Li_{1+x}NiB$ phase. Refined parameters based on synchrotron powder X-ray diffraction data at 295 K are listed. The coordinates of Li and B atoms were not refined but fixed to the values previously determined for *RT*(m)*-LiNiB.

Site	Wyckoff site	*x*	*y*	*z*	U_{iso}, Å^2 × 10^2
RT(m)-$Li_{1+x}NiB$ (*mP*48, $P2_1/c$, *a* = 18.277(1), *b* = 4.86606(5), *c* = 6.1818(2) Å, β = 107.623(1)°, *Z* = 16, R_p = 0.13, R_B = 0.15, *Goof* = 4.08)					
Ni1	4*e*	0.0013(1)	-0.001(3)	0.2277(3)	1.08(2)
Ni2	4*e*	0.2511(1)	-0.002(4)	0.2919(4)	1.08(2)
Ni3	4*e*	0.5007(1)	0.001(3)	0.2946(4)	1.08(2)
Ni4	4*e*	0.7483(1)	-0.003(4)	0.2880(4)	1.08(2)
B1	4*e*	0.01075	0.32589	0.01077	3.3(2)
B2	4*e*	0.26075	0.17411	0.01077	3.3(2)
B1	4*e*	0.51075	0.17411	0.01077	3.3(2)
B2	4*e*	0.76075	0.17411	0.01077	3.3(2)
Li1	4*e*	0.13076	0.25407	0.37955	3.3(2)
Li2	4*e*	0.38076	0.25407	0.37955	3.3(2)
Li2	4*e*	0.63076	0.25407	0.37955	3.3(2)
Li3	4*e*	0.88076	0.25407	0.37955	3.3(2)

Table S3. Atomic coordinates and isotropic equivalent displacement parameters of the *RT(m)*-$Li_{1+x}NiB$ phase. Refined parameters based on synchrotron powder X-ray diffraction data at 100 K are listed. The coordinates of Li and B atoms were not refined but fixed to the values previously determined for *RT*(m)*-LiNiB.

Site	Wyckoff site	*x*	*y*	*z*	U_{iso}, Å^2 × 10^2
RT(m)-$Li_{1+x}NiB$ (*mP*48, *P2₁/c*, *a* = 18.209(1), *b* = 4.86137(3), *c* = 6.1754(2) Å, *β* = 107.542(1)°, *Z* = 8, R_p = 0.12, R_B = 0.15, *Goof* = 3.82)					
Ni1	4*e*	0.0009(1)	-0.001(3)	0.2246(4)	1.07(2)
Ni2	4*e*	0.2509(2)	-0.001(3)	0.2935(4)	1.07(2)
Ni3	4*e*	0.5005(1)	0.002(3)	0.2930(5)	1.07(2)
Ni4	4*e*	0.7484(2)	-0.003(3)	0.2840(5)	1.08(2)
B1	4*e*	0.01075	0.32589	0.01077	3.2(2)
B2	4*e*	0.26075	0.17411	0.01077	3.2(2)
B1	4*e*	0.51075	0.17411	0.01077	3.2(2)
B2	4*e*	0.76075	0.17411	0.01077	3.2(2)
Li1	4*e*	0.13076	0.25407	0.37955	3.2(2)
Li2	4*e*	0.38076	0.25407	0.37955	3.2(2)
Li2	4*e*	0.63076	0.25407	0.37955	3.2(2)
Li3	4*e*	0.88076	0.25407	0.37955	3.2(2)

Table S4. Experimental details and crystallographic data for two structure models of *HT*-$Li_{1+y}NiB$: the idealized monoclinic *HT(m)* and triclinic *HT(t)* with extra Li atoms within the layer. Rietveld refinement was performed on data collected using high resolution synchrotron powder X-ray diffraction (11-BM-B APS).

Empirical formula	*HT(m)*-$Li_{1+y}NiB$*		*HT(t)*-$Li_{1+y}NiB$**	
Formula weight, g/mol	76.45		76.88	
Space group, *Z*	$P2_1/c$, 8		$P1$, 32	
Cell parameters:				
a, Å	3.92591(7)	3.92183(6)	7.8521(1)	7.8438(1)
b, Å	7.5593(1)	7.5492(1)	15.1187(2)	15.0985(3)
c, Å	8.8181(2)	8.7951(1)	8.8181(1)	8.7952(2)
α, °			89.9067(8)	89.8937(8)
β, °	92.6245(7)	92.9962(6)	92.6269(5)	92.9992(6)
γ, °			90.0010(6)	90.0013(6)
V, Å^3	261.42(1)	260.04(1)	1045.71(4)	1040.19(5)
Temperature, K	295	100	295	100
Wavelength, Å	λ = 0.412818			
Step scan	0.001			
2θ° range	1-50			
Program	GSAS II			
R_B	0.16	0.16	0.12	0.14
R_P	0.11	0.12	0.10	0.12
G.O.F.	3.46	3.44	2.98	3.32

*– Further details can be obtained from Cambridge Crystallographic Data Centre/FIZ Karlsruhe deposition service on quoting the depository number CSD-2031389 (100 K) and CSD-2031381 (295 K).

**– Further details can be obtained from Cambridge Crystallographic Data Centre/FIZ Karlsruhe deposition service on quoting the depository number CSD-2031386 (100 K) and CSD-2031377 (295 K).

Table S5. Atomic coordinates and isotropic equivalent displacement parameters of the *HT(m)*-$Li_{1+y}NiB$ phase. Refined parameters based on synchrotron powder X-ray diffraction data at 295 K are listed. The coordinates of Li and B atoms were not refined but fixed to the values obtained from the analysis of interatomic distances and residual electron density peaks.

Site	Wyckoff site	*x*	*y*	*z*	U_{iso}, Å^2 × 10^2
HT(m)-$Li_{1+y}NiB$ (*mP*24, $P2_1/c$, *a* = 3.92591(7), *b* = 7.5593(1), *c* = 8.8181(2) Å, β = 92.6245(7)°, *Z* = 8, R_p = 0.11, R_B = 0.16, *Goof* = 3.46)					
Ni1	4*e*	0.1177(3)	0.7522(1)	0.2419(2)	0.91(2)
Ni2	4*e*	0.3789(3)	0.4560(1)	0.2544(2)	0.91(2)
B1	4*e*	0.12178	0.00862	0.25223	3.8(2)
B2	4*e*	0.38214	0.18698	0.25598	3.8(2)
Li1	2*a*	0	0	0	3.8(2)
Li2	2*c*	0	0	1/2	3.8(2)
Li3	4*e*	0.50195	0.25063	0.00780	3.8(2)

Table S6. Atomic coordinates and isotropic equivalent displacement parameters of the *HT(m)*-$Li_{1+y}NiB$ phase. Refined parameters based on synchrotron powder X-ray diffraction data at 100 K are listed.

Site	Wyckoff site	*x*	*y*	*z*	U_{iso}, $Å^2 \times 10^2$
HT-$Li_{1+y}NiB$ (*mP*24, $P2_1/c$, a = 3.92183(6), b = 7.5492(1), c = 8.7951(1) Å, β = 92.9962(6)°, Z = 8, R_p = 0.12, R_B = 0.16, *Goof* = 3.44)					
Ni1	4*e*	0.1167(3)	0.7500(1)	0.2388(1)	0.68(2)
Ni2	4*e*	0.3783(3)	0.4547(1)	0.2535(2)	0.68(2)
B1	4*e*	0.12178	0.00862	0.25223	3.5(2)
B2	4*e*	0.38214	0.18698	0.25598	3.5(2)
Li1	2*a*	0	0	0	3.5(2)
Li2	2*c*	0	0	1/2	3.5(2)
Li3	4*e*	0.50195	0.25063	0.00780	3.5(2)

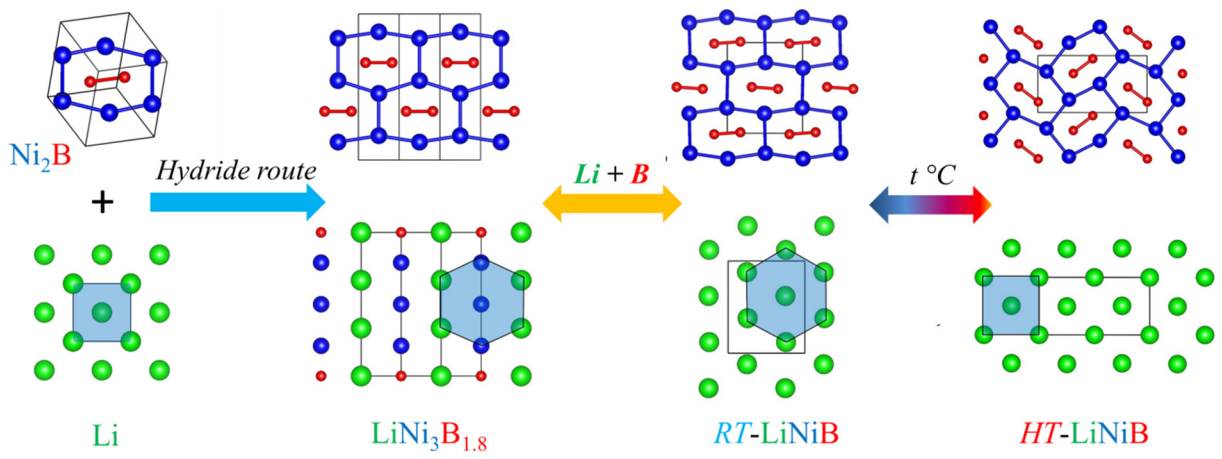

Figure S1. Structural relationship between Li (metal), Ni_2B, $LiNi_3B_{1.8}$, *RT*-LiNiB, *HT*-LiNiB.

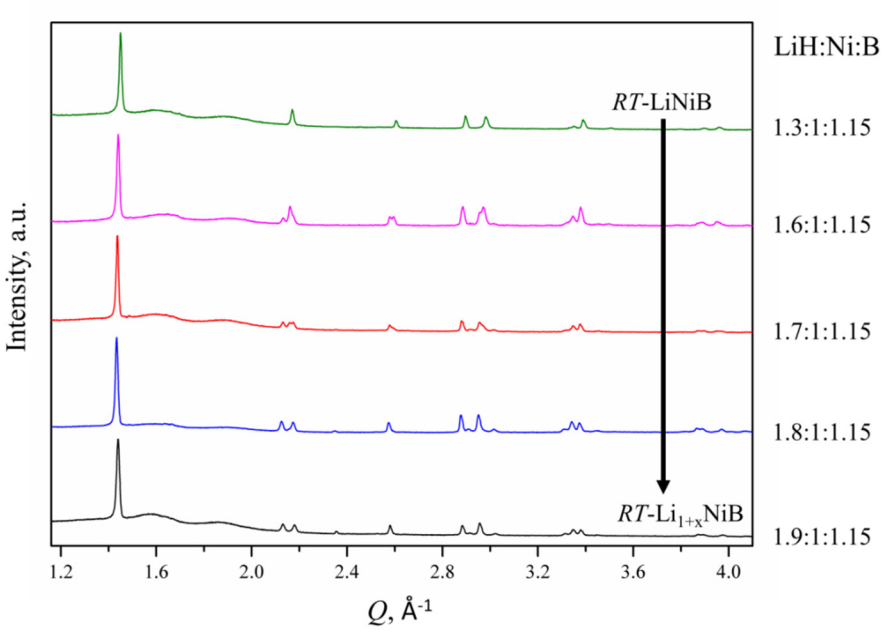

Figure S2. Comparison of X-ray powder diffraction patterns for the samples with the increasing of Li content in loading LiH:Ni:B compositions. Measurements were done in holders for air-sensitive samples and it contributed to the "amorphous" background at ~ 1.6 Å^{-1} *Q* and 1.9 Å^{-1} *Q*. With the increasing of LiH content fraction of *RT*-$Li_{1+x}NiB$ increases and reaches maximum in the sample with LiH:Ni:B = 1.9:1:1.15 loading composition.

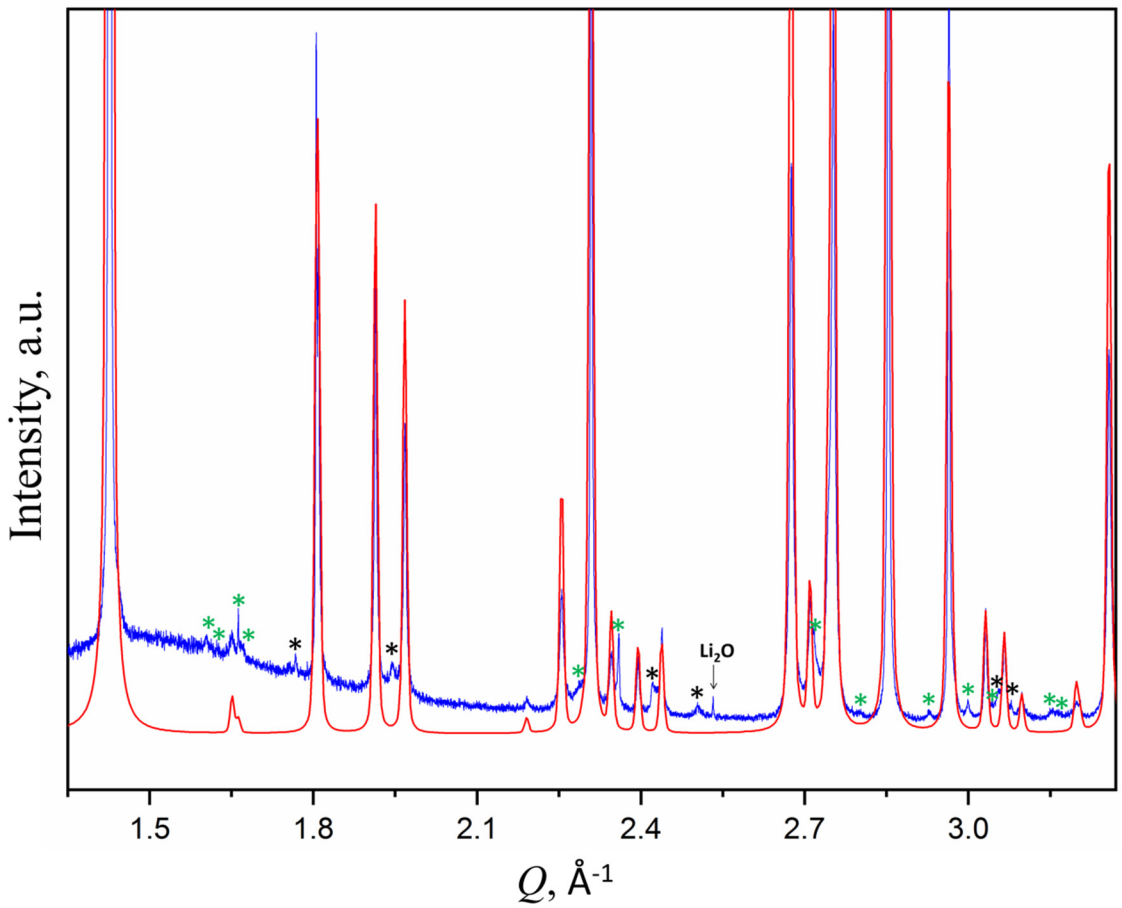

Figure S3. Experimental synchrotron X-ray powder pattern of *HT*-$Li_{1+y}NiB$ and simulated pattern *HT(m)*-$Li_{1+y}NiB$ ($P2_1/c$). Weak satellite peaks that can be accounted by the supercell *HT(t)*-$Li_{1+y}NiB$ ($P1$) are marked with green stars (*), those peaks that cannot be accounted by the supercell denoted with black stars.

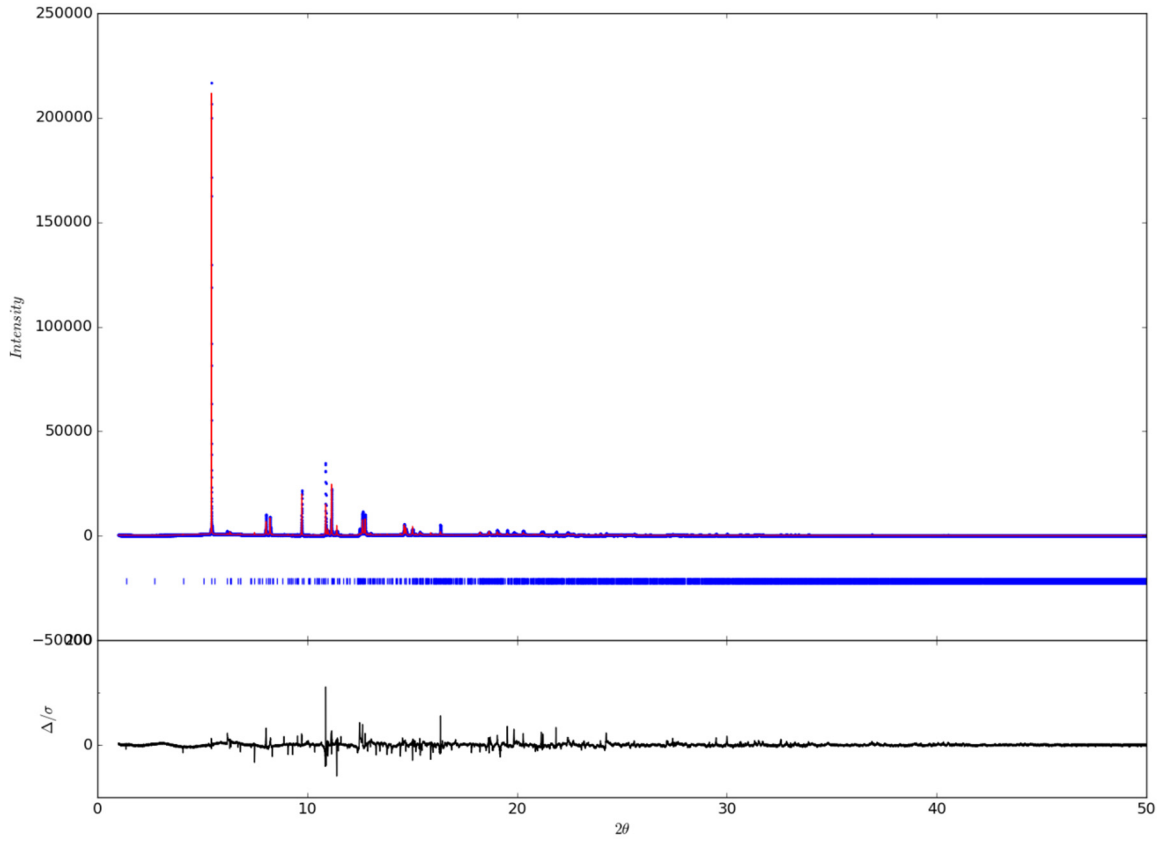

Figure S4. Rietveld refinement plot of synchrotron X-ray powder diffractogram of *RT(m)*-$Li_{1+x}NiB$ ($P2_1/c$) collected at 295 K (experimental powder pattern is in blue, calculated – in red, difference – in black, $R_B = 0.15$, $R_p = 0.13$, *G.O.F.* = 4.08).

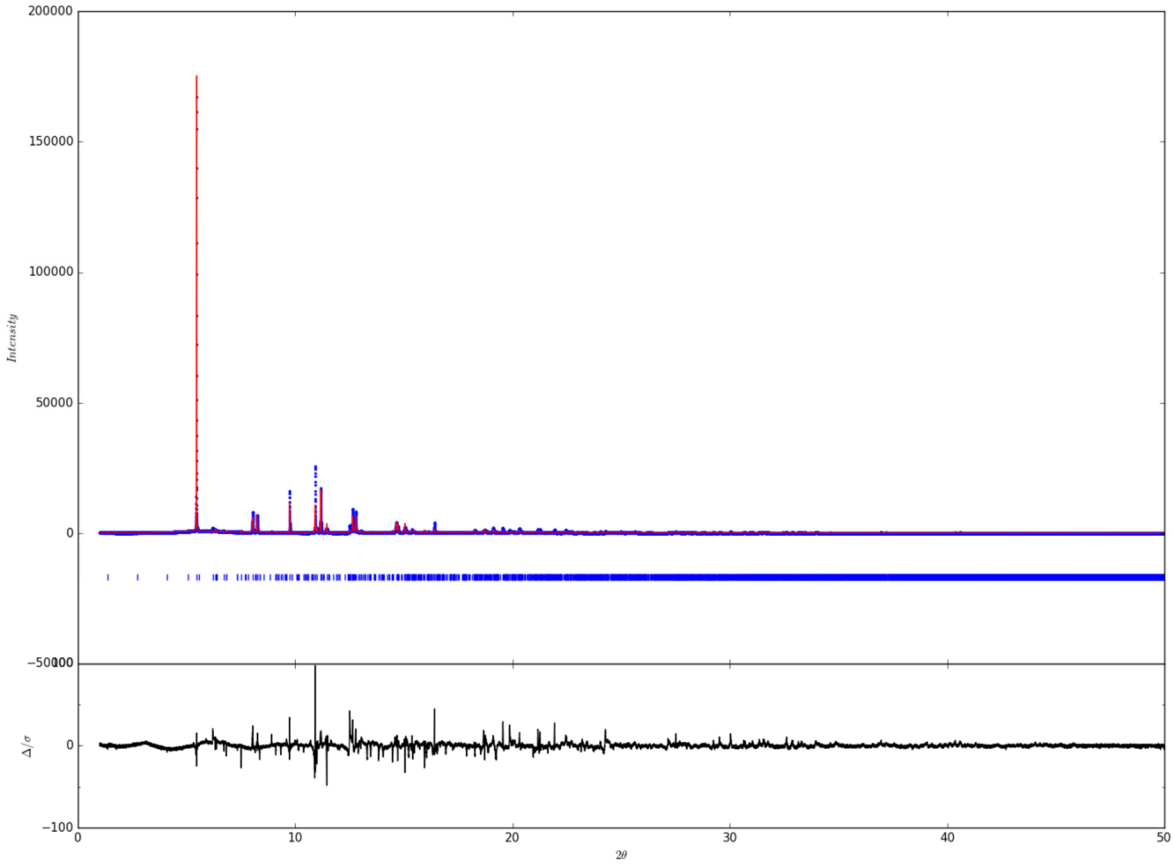

Figure S5. Rietveld refinement plot of synchrotron X-ray powder diffractogram of *RT(m)*-$Li_{1+x}NiB$ ($P2_1/c$) collected at 100 K (experimental powder pattern is in blue, calculated – in red, difference – in black, $R_B = 0.15$, $R_p = 0.12$, *G.O.F.* = 3.82).

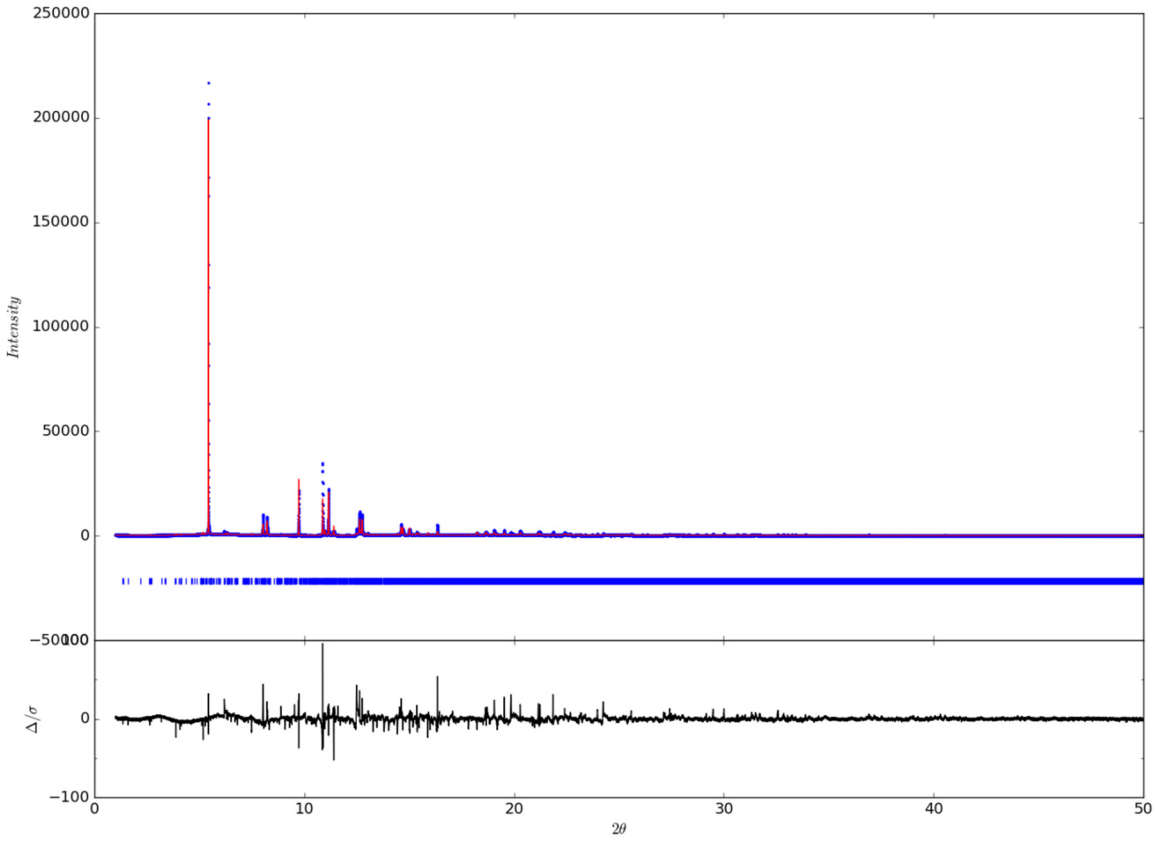

Figure S6. Rietveld refinement plot of synchrotron X-ray powder diffractogram of *RT(t)*-$Li_{1+x}NiB$ (*P*1) collected at 295 K (experimental powder pattern is in blue, calculated – in red, difference – in black, $R_B = 0.15$, $R_p = 0.13$, *G.O.F.* = 3.88).

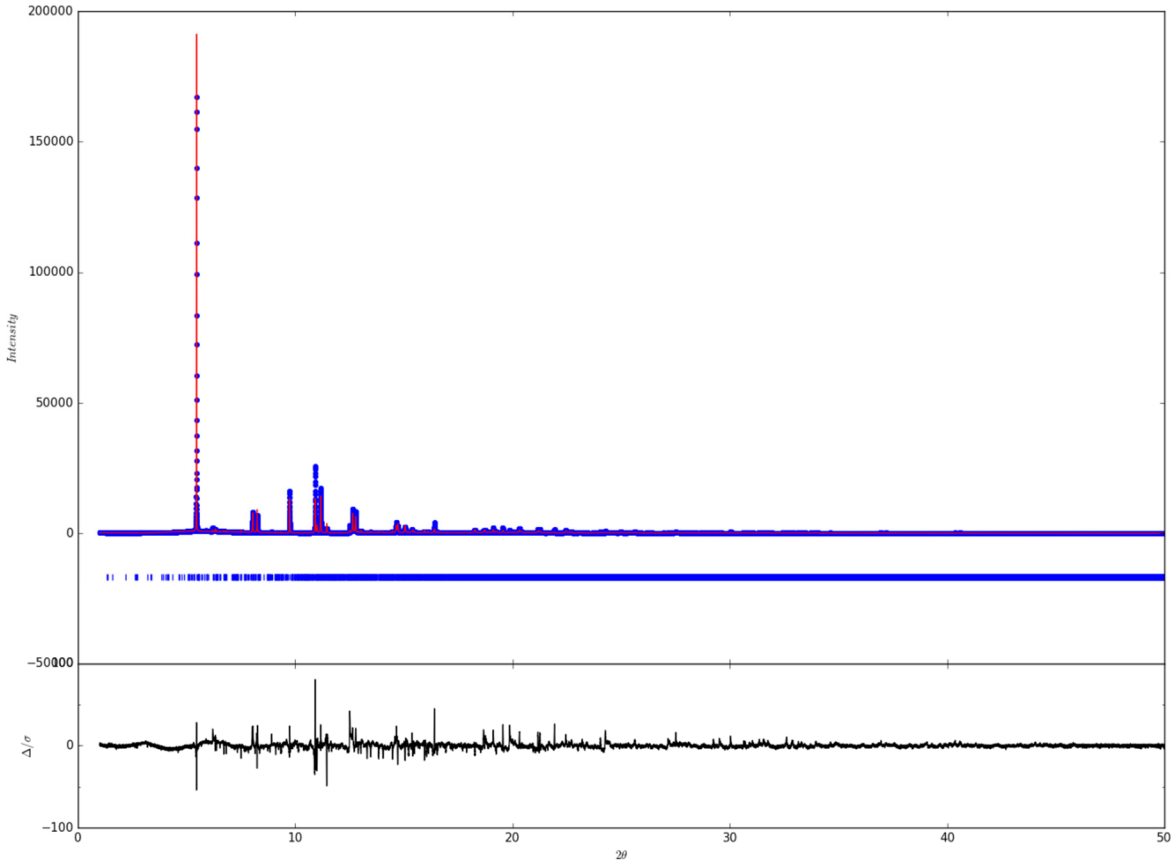

Figure S7. Rietveld refinement plot of synchrotron X-ray powder diffractogram of *RT(t)*-$Li_{1+x}NiB$ (*P*1) collected at 100 K (experimental powder pattern is in blue, calculated – in red, difference – in black, $R_B = 0.14$, $R_p = 0.12$, *G.O.F.* = 3.64).

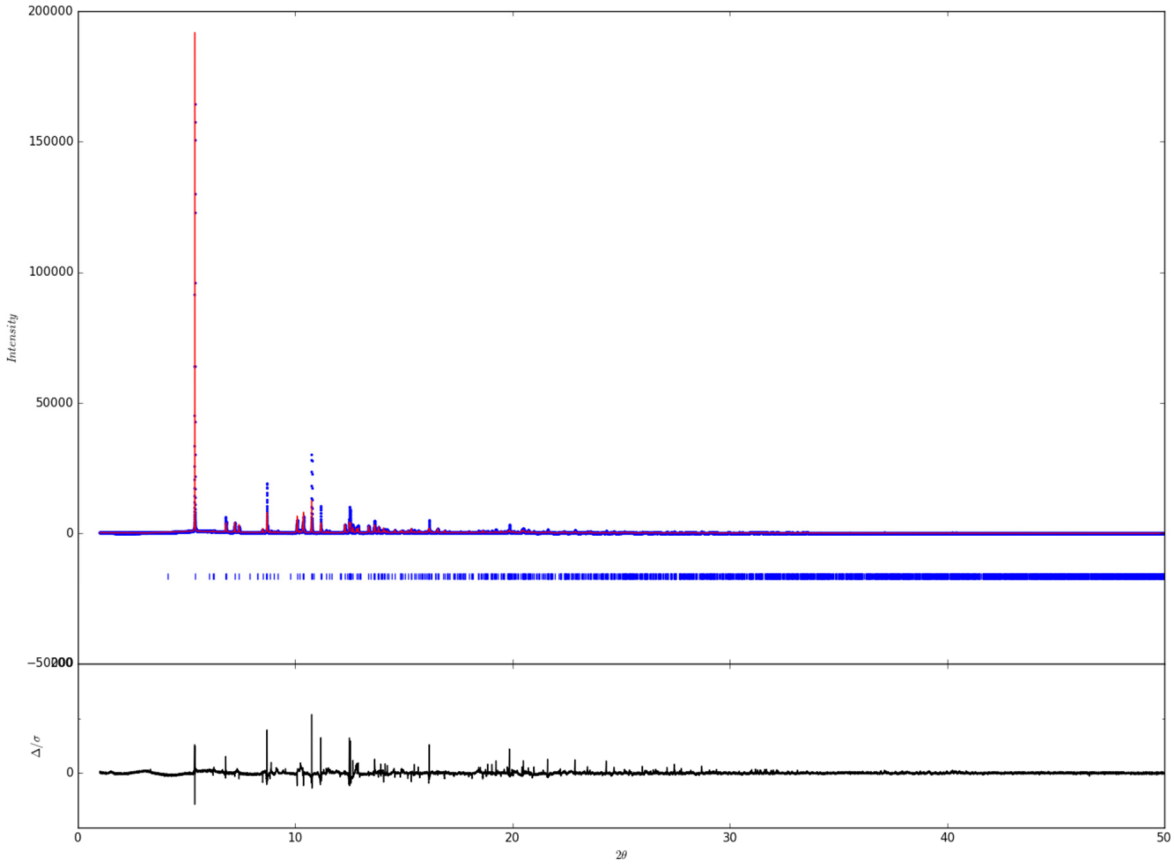

Figure S8. Rietveld refinement plot of synchrotron X-ray powder diffractogram of *HT(m)*-$Li_{1+y}NiB$ ($P2_1/c$) collected at 295 K (experimental powder pattern is in blue, calculated – in red, difference – in black, $R_B = 0.16$, $R_p = 0.11$, *G.O.F.* = 3.46).

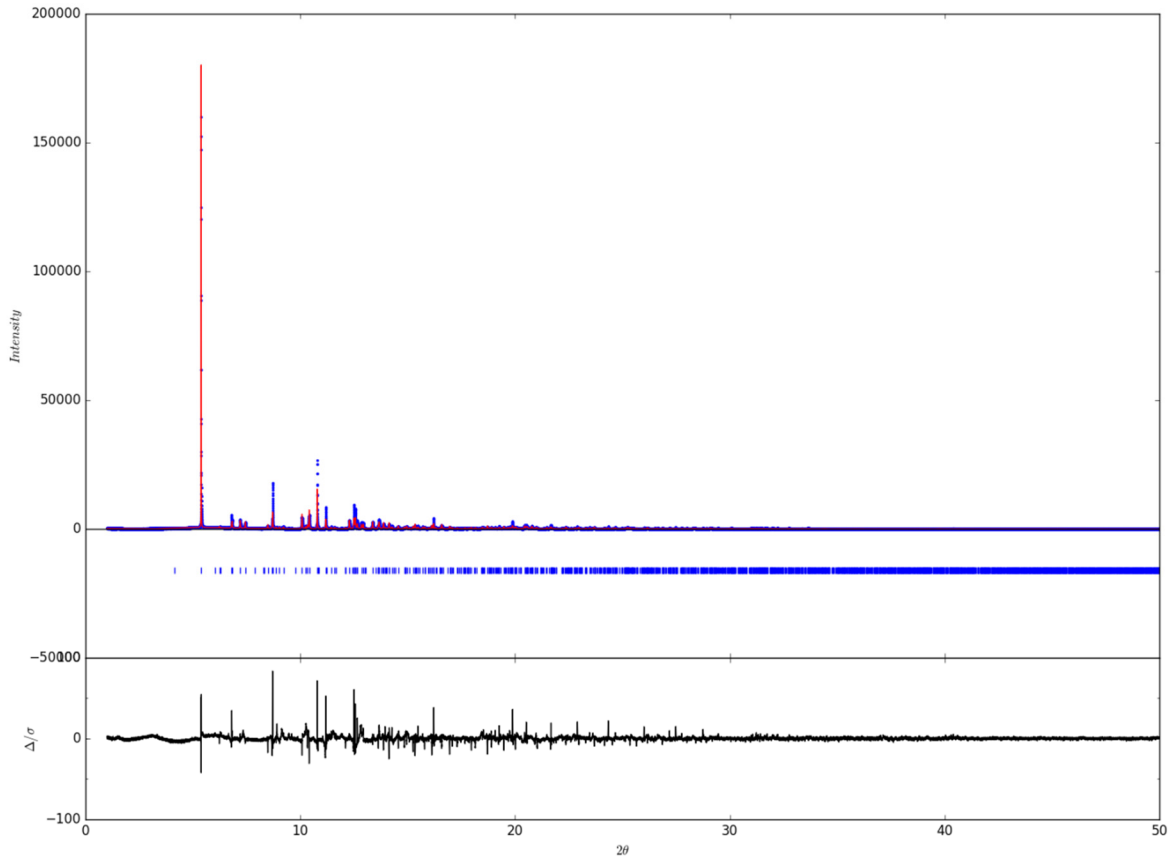

Figure S9. Rietveld refinement plot of synchrotron X-ray powder diffractogram of *HT(m)*-$Li_{1+y}NiB$ ($P2_1/c$) collected at 100 K (experimental powder pattern is in blue, calculated – in red, difference – in black, $R_B = 0.16$, $R_p = 0.12$, *G.O.F.* = 3.44).

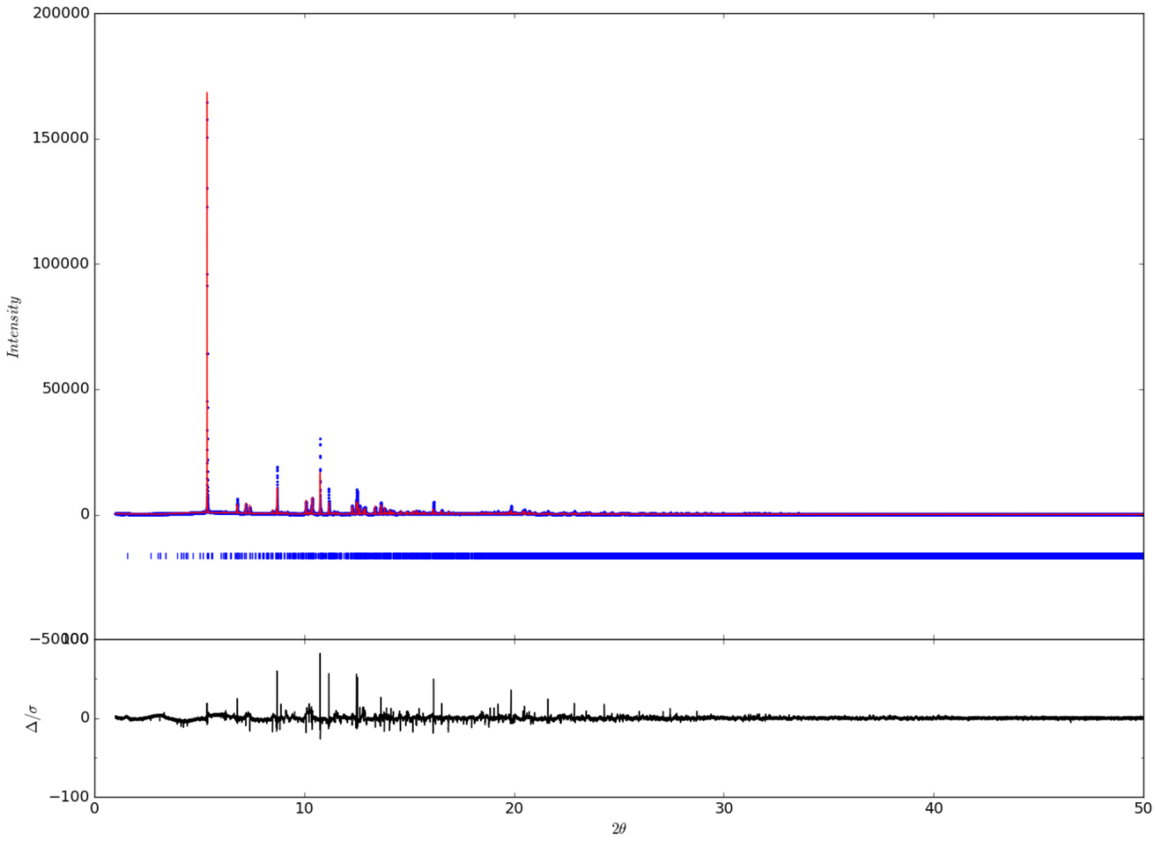

Figure S10. Rietveld refinement plot of synchrotron X-ray powder diffractogram of *HT(t)*-$Li_{1+y}NiB$ (*P*1) collected at 295 K (experimental powder pattern is in blue, calculated – in red, difference – in black, $R_B = 0.12$, $R_p = 0.10$, *G.O.F.* = 2.98).

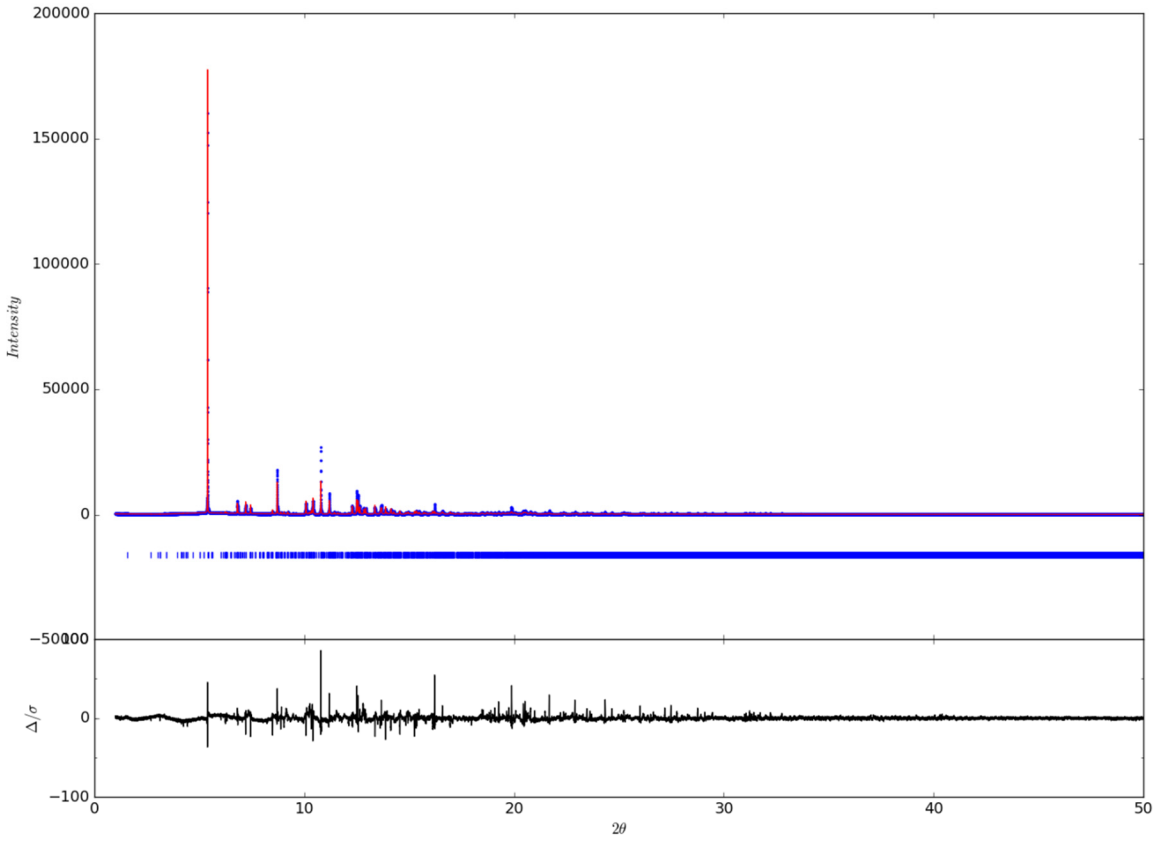

Figure S11. Rietveld refinement plot of synchrotron X-ray powder diffractogram of *HT(t)*-$Li_{1+y}NiB$ (*P*1) collected at 100 K (experimental powder pattern is in blue, calculated – in red, difference – in black, $R_B = 0.14$, $R_p = 0.13$, *G.O.F.* = 3.32).

Table S7. Atomic coordinates and isotropic equivalent displacement parameters of the distorted *HT*-LiNiB phase at 616 K. Refined parameters based on synchrotron powder X-ray diffraction data at 616 K are listed (17-BM APS).

HT-LiNiB (*mP*24, $P2_1/m$, a = 3.9248(2), b = 8.9024(5), c = 7.5549(4) Å, β = 90.023(9)°, Z = 8, R_p = 0.07, R_B = 0.10, *G.O.F.* = 11.7)					
Site	Wyckoff site	x	y	z	U_{iso}, Å^2 × 10^2
Ni1	2*e*	0.469(2)	1/4	0.509(1)	0.2(1)
Ni2	2*e*	0.662(2)	1/4	0.045(1)	0.2(1)
Ni3	2*e*	0.890(2)	1/4	0.741(1)	0.2(1)
Ni4	2*e*	0.155(2)	1.4	0.232(1)	0.2(1)
B1	2*e*	0.18740	1/4	0.00301	3.8(6)
B2	2*e*	0.44764	1/4	0.82447	3.8(6)
B3	2*e*	0.94503	1/4	0.50314	3.8(6)
B4	2*e*	0.68411	1/4	0.32477	3.8(6)
Li1	2*a*	0	0	0	3.8(6)
Li2	2*c*	0	0	1/2	3.8(6)
Li3	4*f*	0.49420	0.50150	0.25054	3.8(6)

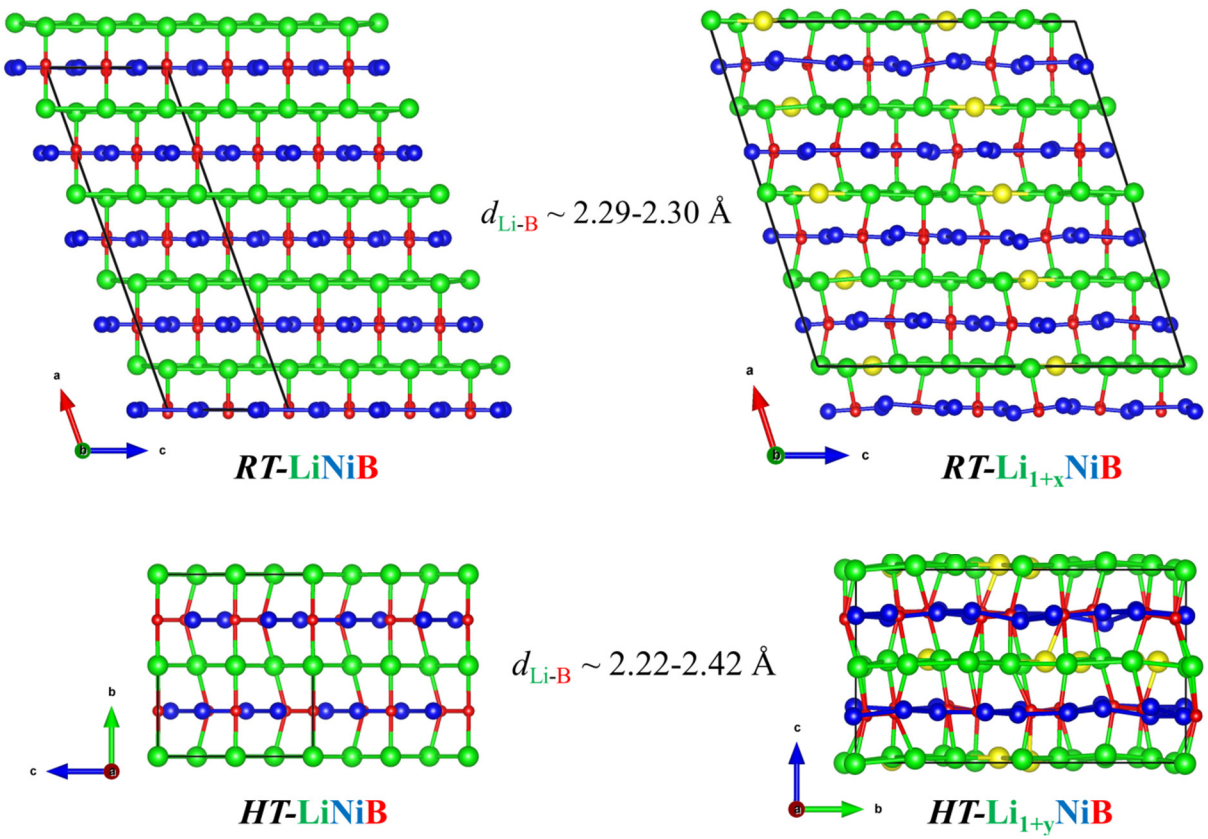

Figure S12. Comparison of the Li-B distances in the structures of parent *RT*-LiNiB, *HT*-LiNiB and Li-enriched *RT*-$Li_{1+x}NiB$ and *HT*-$Li_{1+y}NiB$ polymorphs. Only the bonds within the given cutoff are shown. In the structure of *RT*-LiNiB each Li atom is connected to one B atom (d_{Li-B} ~ 2.29-2.30 Å), while in the structures of *HT*- LiNiB each Li is connected to two B atoms (d_{Li-B} ~ 2.22-2.42 Å). The coordination of most of the Li by B atoms in the Li-enriched *RT*-$Li_{1+x}NiB$ and *HT*-$Li_{1+y}NiB$ polymorphs is similar to that in parent compounds. However, in the structure of *RT*-$Li_{1+x}NiB$ a few Li atoms (shown in yellow) have longer distances (~2.31-2.35 Å) to the adjacent B atoms. Similarly, in the structure of *HT*-$Li_{1+x}NiB$ polymorph a small fraction of Li atoms (shown on yellow) has longer distances to adjacent B atoms (2.43-2.59 Å).

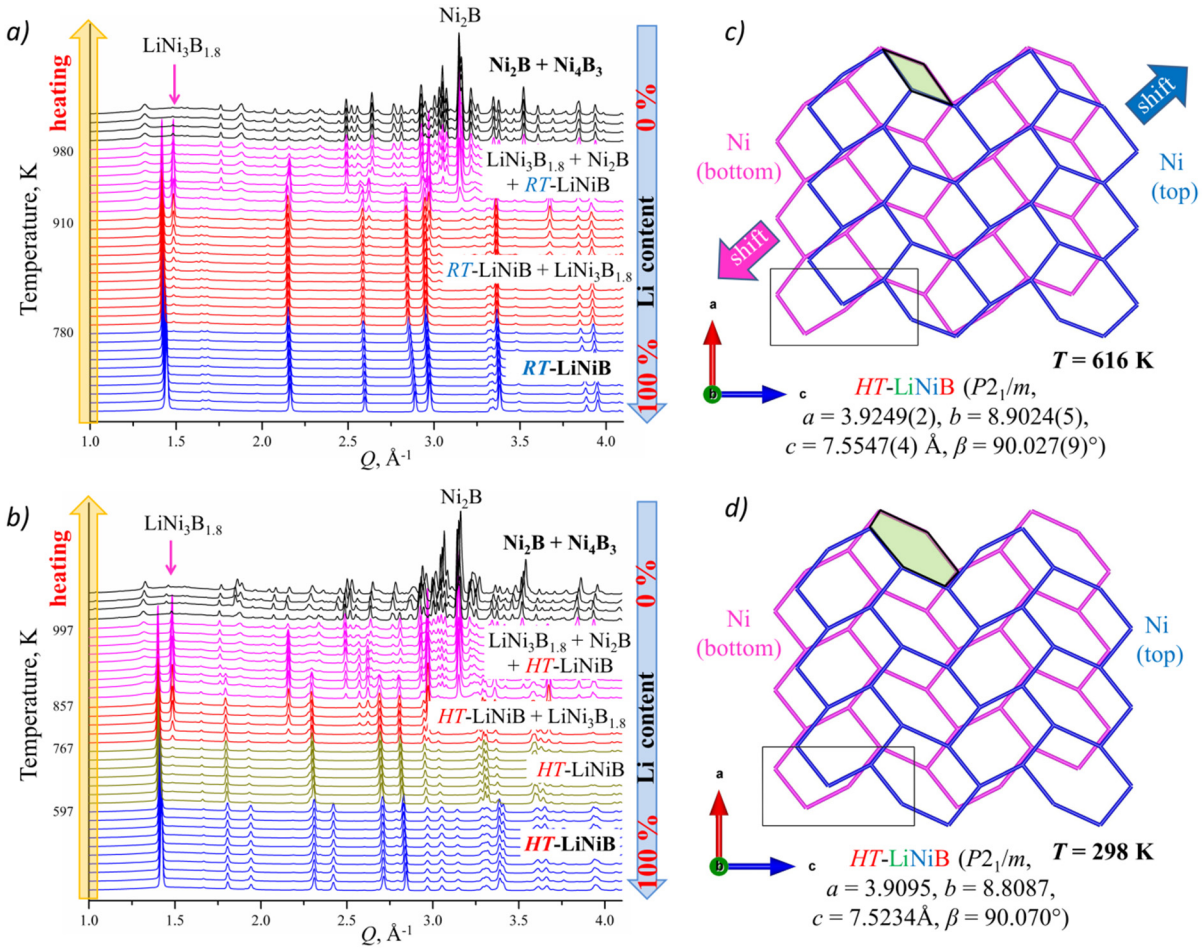

Figure S13. High-temperature *in-situ* X-ray diffraction patterns showing the temperature-driven structural transformation of *RT*-LiNiB (*a*) and *HT*-LiNiB (*b*) compounds. With the increase of temperature Li is being partially leached from the *RT*-LiNiB compound because of reaction with capillary material (SiO_2) resulting in *RT*-LiNiB → $LiNi_3B_{1.8}$ → Ni_2B and Ni_4B_3 transformations. *b) HT*-LiNiB transforms to its distorted variant above 597 K, and further transformations *HT*-LiNiB → $LiNi_3B_{1.8}$ → Ni_2B and Ni_4B_3 occur at higher temperatures. *c)* and *d)* –difference in the structures of [NiB] layers in *HT*-LiNiB and its distorted variant at 616 K.

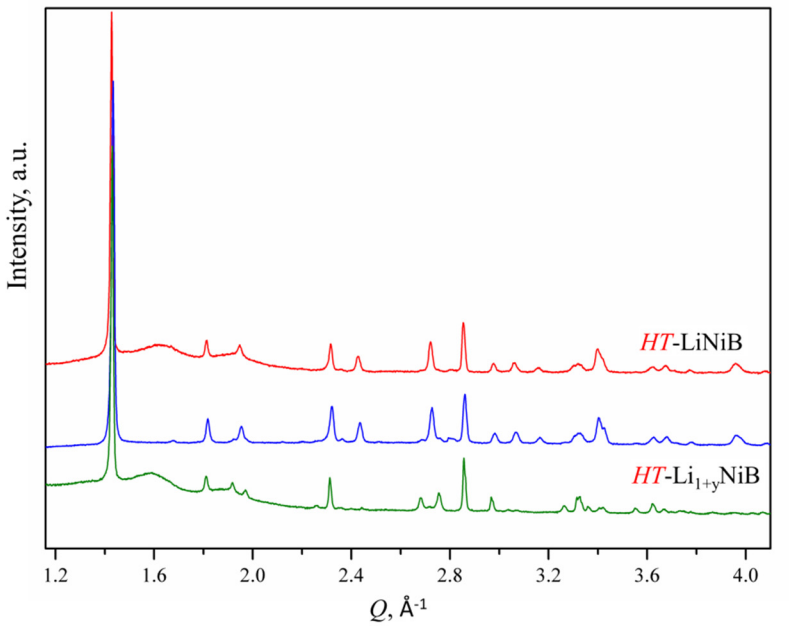

Figure S14. *HT*-$Li_{1+y}NiB$ rapidly transforms in air into *HT*-LiNiB, as evident from the comparison of X-ray powder diffraction patterns of *HT*-$Li_{1+y}NiB$ (green – in air sensitive holder, blue – in open holder) and *HT*-LiNiB (red) compounds. Air sensitive holders provide to the "amorphous" background at ~ 1.6 *Q* and 1.9 *Q*.

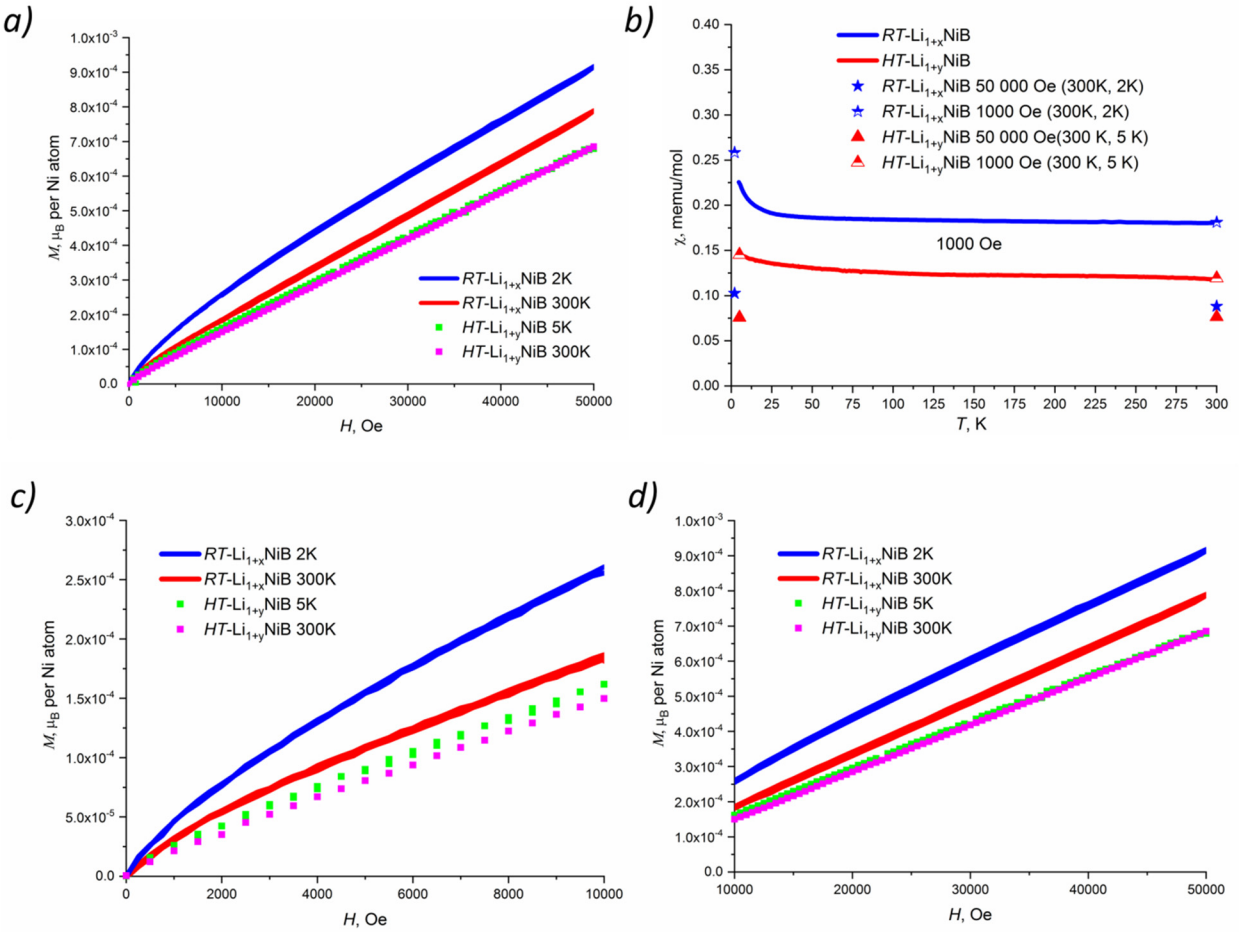

Figure S15. Temperature dependence of magnetization per Ni atom *vs* magnetic field (*a*) and magnetic susceptibility χ *vs. T* (*b*) of *RT*-$Li_{1+x}NiB$ and *HT*-$Li_{1+y}NiB$ polycrystalline samples. A small deviation from the linearity of the *M*(*H*) data at low magnetic fields (*c*), the most pronounced in the *RT*-$Li_{1+x}NiB$ sample at 2 K, could be attributed to some magnetic moment bearing impurity, concentration of which is under the detection limit of X-ray analysis (below 1 %). As a result of this impurity, the 1000 Oe $\chi(T)$ data that is shown for the *RT*-$Li_{1+x}NiB$ phase (*b*) is contaminated by this impurity signal. As such, we have added four additional sets of data points (*b*) inferred from the *M*(*H*) plots to the $\chi(T)$ data for the *RT*-$Li_{1+x}NiB$ phase (star symbols) and *HT*-$Li_{1+y}NiB$ phase (triangle symbols). One set is from the 1000 Oe value of the *M*(*H*) plot, and the other is from the higher field (50000 Oe) slope of the *M*(*H*) plot. These data points provide an estimate of the intrinsic magnetic susceptibility $\chi(T)$ for *RT*-$Li_{1+x}NiB$ and *HT*-$Li_{1+y}NiB$ phases to be in the range of $0.7\text{-}1.2\times10^{-4}$ emu·mol^{-1}. Temperature dependence of magnetization per Ni atom *vs* magnetic field at 10000-50000 Oe is linear as shown in (*d*).